UNNS Substrate Research Program | Working Manuscript

Stellar Boundary Dynamics:

Catastrophic Transition as Routing Between Admissible Structural Regimes

Pilot Corpus: Pre-Supernova Profiles, Light Curves, and Spectral Evolution

Instrument: STRUC-PERC-I v2.5.0

Phase A (2 objects): Zenodo 5556959 · Phase B (6 objects): OSC/AstroCats · Phase C (2 objects): WISeREP

10 STRUC-PERC-I runs · 3 observational layers · 2 pairwise bridges · 1 tri-domain ABC bridge

Status: Pilot manuscript · Date: 2026

Abstract

We present the **Stellar Boundary Dynamics I** corpus: a three-layer structural analysis of core-collapse supernovae processed through STRUC-PERC-I v2.5.0 and the UNNS bridge geometry framework. The corpus spans 10 phase-level structural evaluations distributed across three observational phases: pre-supernova radial profiles (Phase A), post-collapse light curves (Phase B), and post-collapse spectral line-evolution series (Phase C). All 10 STRUC-PERC-I evaluations return FULL-percolation with zero HARD, GIANT, or TAIL outcomes, consistent with the Margin-Confinement Law prediction that identity-preserving physical evolution remains confined to $\mathcal{M}_{\text{adm}}$.

The main contribution is the **ABC tri-domain bridge**, which provides a unified geometric view of how the three observational phases relate in 7-feature bridge-vector space. The bridge classifies the corpus as `A-to-B_contact_with_C_branching`: Phase A (pre-collapse support structure) and Phase B (luminosity relaxation) are weakly separated ($d_{\text{AB}} = 0.401$), while Phase C (spectral redistribution) is strongly separated from both B ($d_{\text{BC}} = 1.287$) and A ($d_{\text{AC}} = 1.365$). This geometry does not support a simple $A \to B \to C$ linear chain; instead it supports a boundary-routing interpretation in which collapse routes structure into non-equivalent downstream admissible regimes.

We formalize this in the **Boundary Routing Conjecture**: a catastrophic transition need not destroy admissibility; instead it may preserve local FULL-percolation while routing structure into multiple downstream regimes that are internally connected but mutually non-equivalent under bridge geometry. Two object archetypes are identified: the *contact-chain* object (SN1993J, branching index = 0.504) and the *branching-anomaly* object (SN2012aw, branching index = 1.470). A key theoretical refinement is established as Proposition 6.2: local FULL-percolation does not imply cross-regime structural equivalence, and the bridge geometry is required to determine whether connected regimes are continuous, weakly separated, or strongly separated. All results are scoped to the pilot corpus.

Contents

1 Introduction

1.1 The boundary-routing question

A central empirical pattern across the UNNS Substrate Research Program is the resistance of physical systems to HARD-class structural fragmentation. The Universal Structural Law (USL) [1], the Percolative Realizability Principle (PRP) [2], and the Margin-Confinement Law (MCL) [3] together establish that admissible systems do not easily escape the interior of $\mathcal{M}_{\text{adm}}$, even under extreme forcing. The 14-domain STRUC-PERC-I baseline (81 evaluations across atomic spectra, nuclear ladders, CMB, cosmic web, seismology, biological fitness landscapes, and others) records zero physical HARD violations.

This consistency raises a question that the existing theory does not address. When a physical system undergoes a *catastrophic boundary event*—a transition in which the pre-event identity cannot be continued—what happens to admissibility? One possibility is that admissibility fails: the post-event state is structurally incoherent. Another possibility is that admissibility persists, but is restructured: the post-event state occupies a different admissible regime, not the same one as the pre-event state.

The present corpus provides a high-energy test of this question using core-collapse supernovae. A stellar collapse is, by any physical measure, a catastrophic event: the pre-collapse stellar interior cannot be continuously deformed into the post-collapse state. It is not an identity-preserving transition in the UNNS sense. The question is therefore: do the post-collapse observables—light curves, spectral evolution—retain structural admissibility? And if they do, is that admissibility a continuation of the pre-collapse structure, or a routing into a different regime?

1.2 Main result

The answer from the pilot corpus is the second possibility. All three observational phases return FULL-percolation. But the tri-domain bridge geometry shows that the three phases are not the same structural regime: A and B are weakly separated, while C is strongly separated from both A and B. This is the **boundary-routing** pattern: the collapse boundary preserves local admissibility while routing structure into non-equivalent downstream regimes.

The key theoretical distinction the corpus motivates is:

> *Internal admissibility (*FULL*-percolation) is not cross-regime equivalence. A system can be admissible in each of several representations while those representations occupy structurally separated positions in bridge geometry.*

This distinction—between being admissible and being in the same admissible regime—is the principal conceptual contribution of this manuscript.

1.3 Relation to prior UNNS manuscripts

The present work extends the UNNS program in a specific direction. Prior manuscripts established the admissibility boundary ($\partial\mathcal{M}_{\text{adm}}$), the Margin-Confinement Law (trajectories cannot cross into HARD), and the Admissible Cluster Geometry (ACG) framework [4] for the internal topology of $\mathcal{M}_{\text{adm}}$. The ACG manuscript introduced the basin-bridgeability relation and structural transport mechanisms across connected admissible regions.

The present corpus provides a pilot instance in which the *generation* of distinct admissi-

ble structural regimes by a catastrophic boundary event is structurally observable within the processed corpus: the pre-boundary regime (Phase A) and the post-boundary regimes (Phase B and Phase C) are produced by the collapse event itself. This complements the ACG static picture of cluster connectivity with a dynamic view of how regimes can arise through boundary-routing.

1.4 Scope and organization

This is a **pilot corpus** manuscript. The corpus spans 10 phase-level evaluations (8 distinct astrophysical targets) across three phases, with two spectral objects in Phase C. All quantitative results are scoped accordingly: structural claims are corpus-level findings, not universal theorems. The formal conjectures in Section 6 are proposed as general principles suggested by the pilot data, not proven from first principles. Cross-domain replication and corpus expansion are deferred to future work (Section 8).

The manuscript is organized as follows. Section 2 sets out the theoretical framework and defines the key concept of an admissible boundary-routing event. Section 3 describes the data sources, objects, and instrument configuration. Section 4 presents percolation results for all three phases. Section 4.2 presents pairwise bridge diagnostics. Section 5 presents the main ABC tri-domain routing geometry. Section 6 states the formal definitions, propositions, theorem, and conjectures. Section 7 places the stellar corpus in the 14-domain STRUC-PERC-I baseline. Section 8 discusses broader theoretical implications. Section 9 concludes.

2 Theoretical Framework

2.1 Admissibility and percolation in the UNNS framework

The Universal Structural Law [1] bounds inversion pressure by vulnerability capacity:

$$\mathrm{inv}(P_\varepsilon;\, L) \;\le\; \nu(V_\varepsilon(L)), \tag{1}$$

where the left side measures how many structural intervals in ladder L are inverted under perturbation scale ε, and the right side measures the vulnerability capacity of the local neighborhood $V_\varepsilon(L)$ in realizability space. A ladder is *admissible* if this inequality holds.

The Percolative Realizability Principle [2] introduces κ-connectivity as a structural coordinate. For a ladder L, the connectivity threshold κ_{conn} is the minimum κ-scale at which a giant connected component containing $\geq 95\%$ of nodes forms. The STRUC-PERC-I instrument returns a four-tier verdict:

- FULL: giant ratio GR $= 1.000$, isolated nodes $= 0$, tail dominance TD $<$ threshold;
- GIANT: GR ≥ 0.95, some isolated nodes;
- TAIL: GR < 0.95, tail-dominated gap structure;
- HARD: structural fragmentation; no dominant giant component.

The Margin-Confinement Law [3] establishes that identity-preserving physical evolutions remain confined to $\mathcal{M}_{\mathrm{adm}}$. The MCL prediction is that any physical system processed under STRUC-PERC-I should return FULL or GIANT under appropriate representation; persistent HARD outcomes signal representation artifacts, not physical failure.

2.2 Structural vectors and bridge geometry

For the bridge analysis, each evaluated object is embedded as a 7-feature normalization-reviewed structural vector derived from STRUC-PERC-I outputs:

$$\mathbf{v}(L) \;=\; \big(\overline{\mathrm{GR}},\; \sigma^2_{\mathrm{GR}},\; \alpha_{\mathrm{aniso}},\; \alpha_{\mathrm{persist}},\; r_{\mathrm{onset}},\; \kappa^{\mathrm{ref}}_{\mathrm{conn}},\; \mathrm{TD}^{\mathrm{ref}}\big), \tag{2}$$

where the features are, respectively: mean giant ratio ($\overline{\mathrm{GR}}$), giant-ratio variance (σ^2_{GR}), bounded anisotropic persistence, admissibility persistence, collapse onset radius, reference κ-connectivity, and reference tail dominance. Superscript "ref" denotes v2 bounded-anisotropic normalization applied to address composition-channel dominance in the Phase A objects.

A bridge between two phases X and Y computes:

$$d(X,Y) \;=\; \big\|\bar{\mathbf{v}}(X) - \bar{\mathbf{v}}(Y)\big\|_2, \tag{3}$$

where $\bar{\mathbf{v}}$ denotes the centroid of structural vectors within a phase. Inter-object pairwise distances $d(\mathbf{v}_i, \mathbf{v}_j)$, closest-pair distances, and furthest-pair distances are also computed.

For the ABC tri-domain bridge, vectors from all three phases are embedded into a common normalization space. The pairwise bridges (A–B and B–C) computed in Sections 4.2 are separate diagnostic runs with within-pair normalization and therefore not directly comparable in absolute scale to the ABC geometry. The ABC result is the authoritative global routing geometry.

2.3 The boundary-routing concept

The central new concept introduced by this manuscript is that of a **boundary-routing event**: a physical transition in which identity-preserving continuation is not possible, but in which structural admissibility persists across the transition through *routing* into downstream admissible regimes.

Formally, we distinguish two qualitatively different post-boundary outcomes:

Fragmentation outcome. The boundary event produces structural incoherence in the post-boundary state. HARD-class verdicts dominate post-boundary evaluations. The system exits $\mathcal{M}_{\mathrm{adm}}$.

Routing outcome. The boundary event produces structurally distinct but internally admissible post-boundary regimes. Each post-boundary observable returns FULL (or GIANT) percolation. However, the post-boundary regimes are not equivalent to the pre-boundary regime, nor necessarily to each other, as measured by bridge geometry.

The routing outcome is theoretically interesting because it separates two properties that might naively be conflated:

$$\text{local admissibility} \;\not\Rightarrow\; \text{cross-regime structural equivalence.} \tag{4}$$

A system can be FULL-percolating in each of its observable representations while those representations are strongly separated in bridge space. Equation (4) is the key structural refinement this corpus motivates.

3 Corpus, Data Sources, and Instrumentation

3.1 Three-layer observational structure

The Stellar Boundary Dynamics I corpus is organized around three distinct observational representations of the same physical class of events (core-collapse supernovae), plus the stellar progenitors that precede them. Each phase constitutes a structural layer in the UNNS bridge framework.

Phase A — Pre-supernova radial profiles. Two pre-SN radial profile objects from Zenodo 5556959 (Laplace et al., stellar evolution simulations using MESA): a 12.09 $M_\odot$ progenitor (`A1_12M`) and a 19.98 $M_\odot$ progenitor (`A2_20M`). Each profile is a terminal snapshot of the stellar interior (not time-resolved), encoding radial variation of temperature, density, composition, specific entropy, and nuclear energy generation rate. Each profile has $n = 64$ ladder rungs after processing. Phase A represents the *pre-boundary support structure* of the stellar system.

Phase B — Post-collapse light curves. Six core-collapse supernovae from the Open Supernova Catalog (OSC/AstroCats): SN1987A, SN1993J, SN1999em, SN2011dh, SN2012aw, and SN2013ej. Each light curve is a multi-band photometric time series processed as a structural ladder encoding temporal brightness evolution across filters. Phase B represents the *luminosity relaxation channel*: the first major post-boundary observable domain.

Phase C — Post-collapse spectral line evolution. Two spectral time series from WISeREP: SN1993J (685 rows) and SN2012aw (198 rows). Each series is a processed sequence of optical spectra encoding spectral-line structure as it evolves across epochs post-explosion. Phase C represents the *spectral redistribution channel*: a second, distinct post-boundary observable domain.

3.2 Data provenance

Table 1: Data sources and processing details for each phase.

Phase	Object(s)	Source	Notes
A	A1_12M, A2_20M	Zenodo 5556959 [7]	`profile_single_M12.09_128net.data`, `profile_single_M19.98_128net.data`; terminal pre-SN snapshots; $n = 64$ rungs each
B	SN1987A – SN2013ej	OSC/AstroCats [8]	Multi-band photometry (UBVRI/BVriz); processed as temporal ladders
C	SN1993J	WISeREP [9]	685-row optical spectral series; line-window proxies as structural features
C	SN2012aw	WISeREP [9]	198-row optical spectral series; line-window proxies as structural features

3.3 Instrument configuration

All percolation evaluations use STRUC-PERC-I v2.5.0. Scale review is performed on all objects prior to bridge analysis; v2 bounded-anisotropic normalization is applied for the bridge runs. The pre-SN profiles require special attention: the composition-channel ratio for `A2_20M` is 254.5× the gap scale, confirming extreme composition-channel dominance in the 20 $M_\odot$ progenitor. V2 normalization is applied to all bridge-comparable structural vectors.

Remark 3.1. Phase A structural vectors are derived from terminal radial snapshots, not from time-resolved stellar evolution tracks. Phase C spectral series encode spectral line-window proxy features, not direct abundance reconstructions. These representational choices are deliberate: they define the structural ladder from which STRUC-PERC-I verdicts are derived, and the bridge geometry is sensitive to which observable representation is used. All results should be interpreted accordingly.

3.4 V2 normalization: scale review and bounded anisotropic persistence

Alpha-application produces a first-pass ($v1$) structural vector for each object. Before bridge comparison, a *scale review* is performed that computes the ratio of each response channel's signal to the gap scale. If any channel dominates by a large factor, the raw $v1$ anisotropic-persistence value becomes unreliable as a cross-object coordinate, because it reflects the dominant channel's scale rather than the object's intrinsic deformation sensitivity.

Scale review is necessary for 9 of the 10 phase-level evaluations in this corpus. The extreme case is `A2_20M`: its composition-channel-to-gap ratio is 254.5×, meaning the composition response dominates the raw alpha-grid scale by more than two orders of magnitude. A1_12M has a composition ratio of 15.5×. In Phase B, most light-curve objects have curvature-channel dominance ranging from 10× to 699,671× (SN2013ej).

The v2 normalization replaces the raw α_{aniso} component with a *bounded anisotropic persistence* value $\alpha_{\text{aniso}}^{\text{bnd}} \in [0, 1]$, computed after capping the dominant channel at the gap scale. This preserves the shape of the structural deformation response while removing the spurious scale amplification from a single dominated channel.

The critical consequence for bridge geometry: v2 normalization affects the bridge distances but does not affect STRUC-PERC-I percolation verdicts. FULL verdicts are determined from the numeric ladder directly, before alpha-application. The bridge distances ($d_{\text{AB}} = 0.401$, etc.) are computed from v2 vectors; the percolation table (Table 2) reflects the numeric ladder results, which are normalization-independent.

Remark 3.2. Scale review is a diagnostic, not a failure flag. An object with scale-review flag means its raw $v1$ anisotropic persistence should not be used directly in bridge comparison. V2 normalization corrects this. The STRUC-PERC-I verdict and κ_{conn} value are unaffected.

4 Percolation Results: Local Structural Admissibility

4.1 Summary: 10/10 FULL-percolation, zero violations

Table 2 presents STRUC-PERC-I v2.5.0 results for all 10 phase-level evaluations across three phases.

All 10 evaluations return FULL-percolation with GR = 1.000, zero isolated nodes, and zero HARD, GIANT, or TAIL outcomes. This is the first STRUC-PERC-I evaluation of catastrophic stellar boundary events in the UNNS program.

4.2 Phase-level structural profiles

The three phases occupy distinct structural tiers.

Phase A (pre-SN profiles): near-immediate connectivity, $\kappa_{\text{conn}} = 1$–2, TD = 0. Both progenitor profiles connect at $\kappa_{\text{conn}} \leq 2$, the lowest tier in the 14-domain STRUC-PERC-

Table 2: STRUC-PERC-I v2.5.0 results for all 10 phase-level evaluations. κ_{conn}: connectivity threshold; TD: tail dominance; n: ladder size; GR: giant ratio. Phase B n values ("—") vary with photometric coverage per object and are not reported in this summary table.

Phase	Object	Type	Verdict	κ_{conn}	TD	n	GR
A	A1_12M	12.09 $M_\odot$ pre-SN	FULL	2	0.000	64	1.000
A	A2_20M	19.98 $M_\odot$ pre-SN	FULL	1	0.000	64	1.000
B	SN1987A	Type II-pec	FULL	0.422	0.000	—	1.000
B	SN1993J	Type IIb	FULL	0.422	0.000	—	1.000
B	SN1999em	Type IIP	FULL	0.178	0.000	—	1.000
B	SN2011dh	Type IIb	FULL	1.000	0.000	—	1.000
B	SN2012aw	Type IIP	FULL	4.400	0.329	—	1.000
B	SN2013ej	Type IIP	FULL	0.316	0.000	—	1.000
C	C1_SN1993J	SN1993J spectra	FULL	201	0.570	685	1.000
C	C2_SN2012aw	SN2012aw spectra	FULL	3992	0.959	198	1.000

I baseline, comparable to biological fitness landscapes ($\kappa_{\text{conn}} = 0.42$–$2.00$) and atmospheric wind fields. Zero tail dominance indicates no extreme outlier gaps in the radial structure. The terminal stellar interior, despite its extreme physical conditions ($\rho_c \approx 10^{10}\,\text{g}\,\text{cm}^{-3}$, $T_c \approx 10^{10}\,\text{K}$), forms a locally homogeneous structural ladder.

Phase B (light curves): $\kappa_{\text{conn}} = 0.18$–$4.40$, TD = 0–0.33. Light curves span the near-immediate to early condensed-matter tier. The range is driven by SN2012aw ($\kappa_{\text{conn}} = 4.40$), which has the highest Phase B connectivity threshold. Tail dominance is zero for five of the six Phase B objects; SN2012aw achieves TD = 0.329, the only non-zero Phase B tail dominance value, consistent with its anomalous routing character across all layers.

Phase C (spectral series): high connectivity, $\kappa_{\text{conn}} = 201$–$3992$, high TD. Phase C exhibits a qualitative jump in structural complexity. Both spectral series require significantly larger κ-scale for percolation, placing them in the CMB/condensed-matter tier of the baseline. SN2012aw spectral series (C2) achieves $\kappa_{\text{conn}} = 3992$ and TD = 0.959, the highest values in this corpus. SN1993J spectral series (C1) achieves $\kappa_{\text{conn}} = 201$ and TD = 0.570.

Observation 4.1. The three-phase κ_{conn} trajectory — Phase A (1–2) → Phase B (0.18–4.40) → Phase C (201–3992) — spans three corpus tiers from the same family of physical objects. This is consistent with the Phase Mapping finding that representation is the dominant structural variable: the same physical event class occupies different structural coordinates depending on which observable channel is used.

Figure 1 illustrates the cross-phase escalation of κ_{conn} and TD for all 10 phase-level evaluations. Every evaluation returns FULL-percolation; the figure shows that this verdict is achieved across an enormous range of structural scales.

This section presents pairwise bridge runs for A–B and B–C. These are **pairwise diagnostic runs** with within-pair v2 normalization; they are not the authoritative global routing geometry. The canonical distances are from the ABC bridge (Section 5): $d_{\text{AB}} = 0.401$, $d_{\text{BC}} = 1.287$, $d_{\text{AC}} = 1.365$. The pairwise values ($d_{\text{AB}}^{\text{pw}} = 0.584$, $d_{\text{BC}}^{\text{pw}} = 1.318$) use a different normalization space and are not directly comparable to the ABC centroid distances in absolute scale.

Remark 4.2 (Pairwise bridges vs. ABC tri-domain bridge). The A–B and B–C **pairwise**

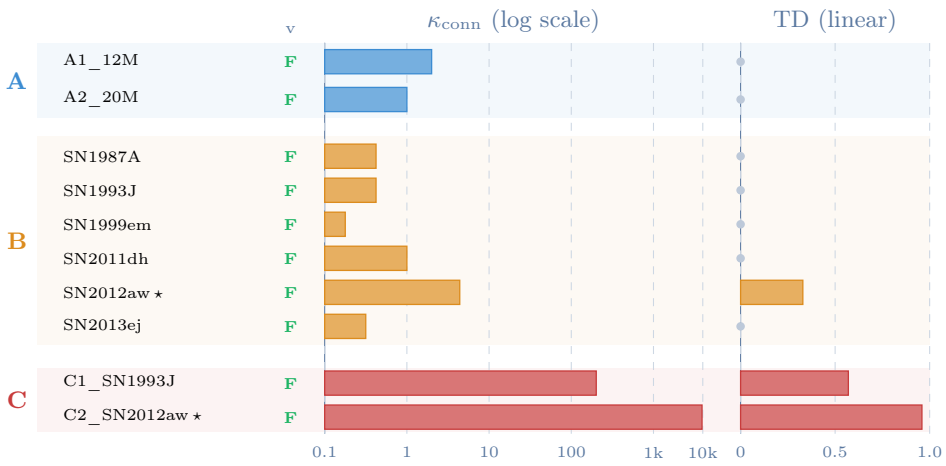

Figure 1: κ_{conn} (left panel, log scale) and TD (right panel, linear) for all 10 phase-level evaluations. Column "v" shows the percolation verdict: **F** = FULL for all 10. Blue = Phase A, amber = Phase B, red = Phase C; ⋆ marks the SN2012aw anomaly chain. All evaluations return FULL while κ_{conn} spans five decades (0.18 to 3,992) and TD escalates from zero in Phase A to 0.570–0.959 in Phase C. The jump between Phase B and Phase C is abrupt: the largest Phase B κ_{conn} is 4.4; the smallest Phase C κ_{conn} is 201.

bridges embed only two domains at a time and normalize within that pair. The **ABC** bridge embeds all three domains jointly in a unified normalization space. Because the normalization reference differs, pairwise distances and ABC distances are not interchangeable:

- Pairwise A–B: $d_{\text{AB}}^{\text{pw}} = 0.584$ (diagnostic, within-pair normalization);
- ABC A–B: $d_{\text{AB}} = 0.401$ (authoritative, unified tri-domain normalization).

Both results agree on the qualitative conclusion: A and B are weakly separated, while B–C and A–C are strongly separated. The ABC bridge is the single source of truth for the global routing geometry.

4.3 A–B pairwise bridge: pre-collapse to light curve

The A–B pairwise bridge embeds both Phase A and Phase B objects in a common v2 normalization of the 7-feature bridge-vector space. The centroid distance is $d_{\text{AB}}^{\text{pw}} = 0.584$ (weak separation).

The centroid-level feature shifts from A to B are driven primarily by:

- `mean_GR`: +0.296 (giant ratio rises in light curves);
- `anis. persist. (bounded)`: +0.305 (light curves more deformation-sensitive);
- `collapse_onset_radius`: +0.250 (geometric onset coordinate shifts when moving from radial profiles to temporal brightness trajectories).

Object-level results identify `A2_20M` ($20\,M_{\odot}$) as the nearest A-object to the B centroid (structural attractor for the majority of post-collapse light curves) and SN1993J as the nearest B-object to the A centroid (closest post-collapse event to the pre-collapse structural domain).

4.4 B–C pairwise bridge: light curve to spectral evolution

The B–C pairwise bridge gives $d_{\text{BC}}^{\text{pw}} = 1.318$ (strong separation). This is more than twice the A–B pairwise distance, establishing that the light-curve-to-spectral-series transition involves a larger structural displacement than the pre-collapse-to-light-curve transition.

The dominant feature shifts from B to C are:

- `tail_dominance_ref`: +0.740 (largest shift; spectral layer is heavily tail-dominated in C);
- `kappa_connect_ref`: +0.525 (large κ jump; spectra require a much larger connectivity scale);
- `admissibility_persist`: −0.584 (C admissibility persistence collapses, dominated by SN2012aw extreme values in C2).

Object-matched coherence test. When both B and C objects have spectral counterparts, we can test whether the matched pair (same SN in both layers) is closer in bridge-vector space than the cross-matched pair. Results:

- **SN1993J**: B_SN1993J ↔ C1_SN1993J is the nearest neighbor of C1 in Phase B. Coherent: the light curve and spectrum of SN1993J are structurally consistent.
- **SN2012aw**: B_SN2012aw ↔ C2_SN2012aw has $d = 1.923$; C1_SN1993J is closer to B_SN2012aw ($d = 0.648$) than its own spectral counterpart. Incoherent: SN2012aw's spectral layer adds structural information that is not a continuation of its light-curve structure.

This object-matched incoherence for SN2012aw is the first appearance of what will emerge as the *branching-anomaly archetype* (Section 5).

5 ABC Tri-Domain Routing Geometry

5.1 Main result: global routing classification

The ABC tri-domain bridge embeds all 10 phase-level evaluations (Phases A, B, and C) in a unified v2 normalization space and computes all three centroid distances and the global routing classification.

Table 3: ABC tri-domain bridge: centroid distances and routing classification. All values from v2 normalization-reviewed structural vectors.

Pair	Centroid distance	Classification	Interpretation
A–B	0.401	weak separation	Pre-collapse profiles and light curves are structurally close; inherited routing
B–C	1.287	strong separation	Light curves and spectral series are structurally distinct; different post-boundary regime
A–C	1.365	strong separation	Spectral series are far from pre-collapse profiles; deep routing displacement
Global classification:			`A_to_B_contact_with_C_branching`

The branching indices quantify how much farther C is from the A–B axis:

$$d_{\mathrm{BC}} - d_{\mathrm{AB}} = 1.287 - 0.401 = 0.886, \tag{5}$$

$$d_{\mathrm{AC}} - d_{\mathrm{AB}} = 1.365 - 0.401 = 0.964. \tag{6}$$

Both are positive and substantial, confirming that C does not lie on an $A \to B \to C$ linear path. The ordering $d_{\mathrm{AB}} \ll d_{\mathrm{BC}} \approx d_{\mathrm{AC}}$ is the signature of the routing geometry: B inherits weakly from A, while C branches into a distinct regime equally removed from both A and B.

Figure 2 illustrates this geometry.

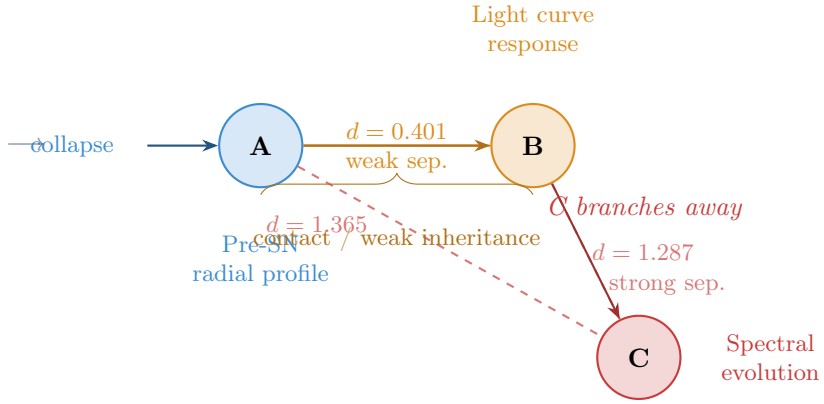

Figure 2: ABC routing geometry. Phase A (pre-collapse profiles) and Phase B (light curves) are weakly separated ($d = 0.401$; amber solid line). Phase C (spectral evolution) is strongly separated from both B ($d = 1.287$) and A ($d = 1.365$; red dashed lines), constituting an independent post-collapse regime. The global classification is `A_to_B_contact_with_C_branching`.

5.2 Domain-pair distance matrix

Table 4 provides the complete domain-pair distance matrix including closest and furthest object pairs for each domain combination.

Table 4: Domain-pair distance matrix for the ABC bridge (v2 unified vectors). Closest and furthest individual object pairs are shown for each domain combination.

Pair	Centroid d	Class	Closest pair		d	Furthest pair		d
A–B	0.401	weak sep.	A2_20M B_SN1993J	↔	0.150	A2_20M B_SN1987A	↔	1.393
B–C	1.287	strong sep.	B_SN2012aw C1_SN1993J	↔	0.543	B_SN1987A C2_SN2012aw	↔	2.501
A–C	1.365	strong sep.	A2_20M C1_SN1993J	↔	0.661	A1_12M C2_SN2012aw	↔	2.449

The closest B–C pair is cross-matched (B_SN2012aw ↔ C1_SN1993J, $d = 0.543$), not the matched SN2012aw pair, confirming the incoherence finding from Section 4.2.

5.3 Object chains: contact-chain and branching-anomaly archetypes

Two individual-object chains can be traced end-to-end through the ABC bridge (objects sharing SN identifiers across two or more phases):

SN1993J chain: A2_20M → B_SN1993J → C1_SN1993J.

$$\begin{aligned} d(\text{A2\_20M, B\_SN1993J}) &= 0.150, \\ d(\text{B\_SN1993J, C1\_SN1993J}) &= 0.654, \\ d(\text{A2\_20M, C1\_SN1993J}) &= 0.661, \\ \text{BI(SN1993J)} &= d_{\text{BC}} - d_{\text{AB}} = 0.504. \end{aligned}$$

The chain is compact: $d_{\text{AC}} \approx d_{\text{BC}}$ (nearly equilateral), indicating that C is nearly equidistant from A and B. The A–B step ($d = 0.150$) is the smallest object-pair distance in the entire

corpus. SN1993J demonstrates that the stellar boundary can be traversed with near-linear structural inheritance across all three observable layers.

SN2012aw chain: A2_20M → B_SN2012aw → C2_SN2012aw.

$$\begin{aligned} d(\text{A2\_20M}, \text{B\_SN2012aw}) &= 0.438, \\ d(\text{B\_SN2012aw}, \text{C2\_SN2012aw}) &= 1.908, \\ d(\text{A2\_20M}, \text{C2\_SN2012aw}) &= 2.009, \\ \text{BI}(\text{SN2012aw}) &= 1.470. \end{aligned}$$

The chain is elongated and strongly branching. The A–B step ($d = 0.438$) already places SN2012aw further from the A domain than SN1993J's entire A–C distance. The B–C step ($d = 1.908$) is the largest matched-pair step in the corpus, nearly 3× SN1993J's B–C step ($d = 0.654$). SN2012aw's spectral layer is structurally more displaced from the pre-collapse progenitor than any other object in the corpus.

The branching-index contrast (BI = 0.504 vs BI = 1.470, ratio 2.9×) establishes SN1993J and SN2012aw as representatives of two structural routing archetypes. Figure 3 illustrates both chains.

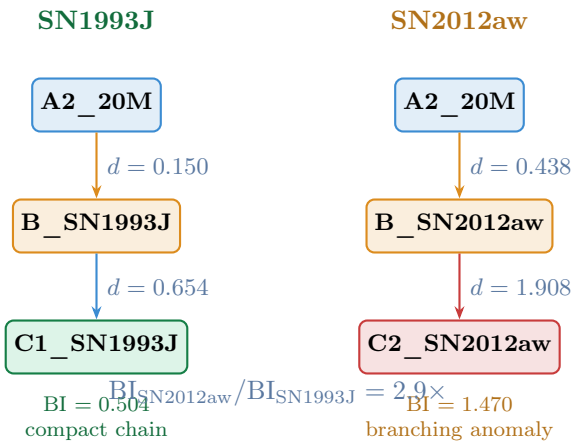

Figure 3: Object chain comparison. Left: SN1993J contact chain, with compact A–B step ($d = 0.150$, corpus minimum) and equilateral geometry (BI = 0.504). Right: SN2012aw branching-anomaly chain, with elongated A–B step and a B–C step ($d = 1.908$) that is 3× larger (BI = 1.470). Both chains terminate with FULL-percolation at every node.

5.4 Orthogonal structural drivers at each transition

A feature-level analysis of the ABC centroid shifts identifies different structural coordinates as the primary drivers of each inter-phase transition.

The transition drivers are orthogonal:

- **A → B** is anchored in `collapse_onset_radius` (+0.250): the geometric onset coordinate that shifts when moving from radial profiles to temporal brightness trajectories.
- **B → C** is anchored in `tail_dominance` (+0.740) and `kappa_connect` (+0.525): the connectivity-depth and gap-outlier dimensions characteristic of how heterogeneous the spectral line landscape is.

Table 5: Leading feature drivers at each transition. Centroid shifts (A→B and B→C) from the ABC unified vector space.

Feature	A centroid	B centroid	C centroid	A→B Δ	B→C Δ
`tail_dominance_ref`	0.000	0.057	0.797	+0.057	+0.740
`kappa_connect_ref`	0.000	0.000	0.525	≈ 0	+0.525
`admissibility_persist`	0.593	0.549	0.033	−0.044	−0.516
`collapse_onset_radius`	0.000	0.250	0.000	+0.250	−0.250
`mean_GR`	≈ 0	≈ 0	0.500	≈ 0	+0.500

This orthogonality implies that the boundary event is not a single structural deformation. It activates different structural variables at different observable transitions, providing mechanistic grounding for why A–B and B–C register as distinct transitions rather than steps along one deformation path.

6 Formal Layer

This section formalizes the main theoretical contributions as a definition, a proposition, a pilot-corpus theorem, and two conjectures. All scope qualifications apply: the proposition and theorem are corpus-scoped empirical statements, while the conjectures are proposed general principles requiring broader replication.

Definition 6.1 (Admissible Boundary-Routing Event)**.** A physical system with multiple observational representations $\{L_1, L_2, \ldots, L_k\}$ of a transition event undergoes an *admissible boundary-routing event* if:

(i) each ladder L_i is internally FULL-percolating under STRUC-PERC-I evaluation;

(ii) at least two layers L_i, L_j are structurally non-equivalent under bridge geometry, i.e. $d\big(\bar{\mathbf{v}}(L_i), \bar{\mathbf{v}}(L_j)\big) > \theta_{\text{sep}}$;

(iii) the post-boundary observables produce a routed cluster geometry rather than a single linear successor chain.

The global routing classification (`A_to_B_contact_with_C_branching`, `linear_chain`, etc.) describes the topological type of the routing geometry.

The Stellar Boundary Dynamics I corpus satisfies all three conditions of Definition 6.1: all 10 phase-level evaluations are FULL, the ABC bridge gives $d_{\text{BC}} = 1.287$ and $d_{\text{AC}} = 1.365$ (both strong separation), and the global classification is `A_to_B_contact_with_C_branching`.

Proposition 6.2 (Internal Admissibility Is Not Cross-Regime Equivalence)**.** *In the Stellar Boundary Dynamics I corpus,* FULL*-percolation in each of Phases A, B, and C does not imply structural equivalence of those phases under bridge geometry.*

$$\text{FULL}(A) \wedge \text{FULL}(B) \wedge \text{FULL}(C) \not\Rightarrow A \approx_{\text{bridge}} B \approx_{\text{bridge}} C. \tag{7}$$

Specifically, while all three phases are internally admissible, the ABC bridge gives $d_{\text{AB}} = 0.401$ (weak separation), $d_{\text{BC}} = 1.287$ (strong separation), and $d_{\text{AC}} = 1.365$ (strong separation).

Proof. By direct computation in the v2 unified normalization space (Table 3). The FULL-percolation result holds for all 10 evaluations (Table 2); the bridge distances are not compatible with a single admissible regime, as strong separation ($d > 1.0$) is exhibited in two of

three domain pairs. □

Remark 6.3. Proposition 6.2 establishes that STRUC-PERC-I percolation verdicts and bridge geometry measure different properties of a multi-layer system. Percolation measures *local structural viability* within a representation. Bridge geometry measures *regime relation* between representations. Both are required for a complete structural analysis of a multi-observable physical event.

Theorem 6.4 (Stellar Boundary Routing, Pilot-Corpus Empirical Theorem)**.** *In the Stellar Boundary Dynamics I pilot corpus, the three observed phases — pre-supernova radial profiles (A), post-collapse light curves (B), and post-collapse spectral time series (C) — each remain internally* FULL*-percolating, while the unified ABC bridge classifies the tri-domain geometry as* `A_to_B_contact_with_C_branching`*.*

Therefore, within this processed pilot corpus, stellar collapse is structurally represented not as a single $A \to B \to C$ linear chain, but as $A \to B$ weak inheritance with C branching into a distinct admissible spectral regime.

Proof. Percolation: Table 2 gives FULL for all 10 evaluations. Bridge geometry: Table 3 gives $d_{\mathrm{AB}} = 0.401 < d_{\mathrm{BC}} = 1.287 \approx d_{\mathrm{AC}} = 1.365$, with $d_{\mathrm{BC}} - d_{\mathrm{AB}} = 0.886 > 0$ and $d_{\mathrm{AC}} - d_{\mathrm{AB}} = 0.964 > 0$. The ordering $d_{\mathrm{AB}} \ll d_{\mathrm{BC}} \approx d_{\mathrm{AC}}$ establishes that C is approximately equidistant from A and B, and much further from both than A and B are from each other. This is the defining signature of the `A_to_B_contact_with_C_branching` classification. □

Remark 6.5. Theorem 6.4 is an *empirical theorem* scoped to the pilot corpus: it is a derivable consequence of the measured bridge distances, not a universally proven claim about all stellar collapses. Generalization requires corpus expansion (additional progenitor masses, SN subtypes, and spectral series).

Conjecture 6.6 (Boundary Routing Conjecture)**.** A catastrophic transition in a physically realized system need not destroy admissibility. Instead, the transition may preserve local FULL-percolation (or near-FULL connectivity) in each post-boundary observable representation, while routing the system into multiple downstream structural regimes that remain internally connected but are mutually non-equivalent under bridge geometry. In compact form:

$$\begin{aligned} \text{catastrophic transition} &\neq \text{necessary structural fragmentation;} \\ \text{catastrophic transition} &= \text{possible routing among admissible regimes.} \end{aligned}$$

Conjecture 6.7 (Contact-Chain / Branching-Anomaly Dichotomy)**.** Within a boundary-routing corpus, objects separate into at least two structural archetypes:

(i) *Contact-chain objects*, which preserve compact cross-layer geometry (small branching index, $d_{\mathrm{AC}} \approx d_{\mathrm{BC}}$);

(ii) *Branching-anomaly objects*, whose later observable layers separate sharply from the A–B entry path (large branching index, escalating cross-layer displacement).

Both archetypes remain internally FULL-percolating; the distinction is in routing geometry, not in local admissibility. In the pilot corpus, SN1993J (BI = 0.504) is a contact-chain object

and SN2012aw (BI = 1.470) is a branching-anomaly object.

7 Corpus Placement and Cross-Domain Context

The 14-domain STRUC-PERC-I baseline provides a reference scale against which the stellar corpus can be placed. Figure 4 shows the κ_{conn} range of all three stellar phases alongside selected baseline domains.

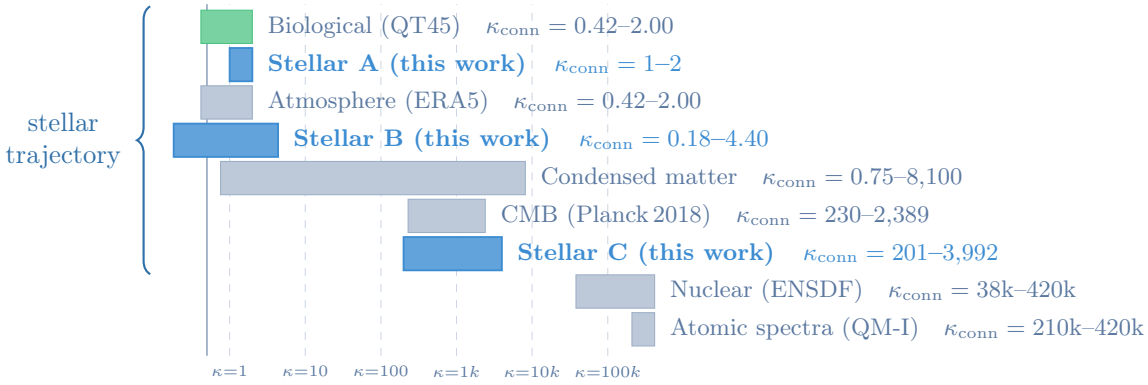

Figure 4: κ_{conn} tier placement of the stellar corpus against the 14-domain STRUC-PERC-I baseline (log scale; blue bars = stellar, gray = baseline). Phase A lands in the biological/atmospheric tier; Phase B spans near-immediate to low condensed-matter range; Phase C approaches the CMB/condensed-matter tier. The cross-tier trajectory is governed by representation, not by the underlying physics.

The three-tier trajectory from Phase A to Phase C within a single physical object family is consistent with the Phase Mapping finding that representation is the dominant structural variable. The same collapse event, observed through radial profiles, photometric light curves, and optical spectra, occupies different structural coordinates in realizability space — not because the physics differs, but because the structural ladder that each observable representation constructs differs.

8 Discussion

8.1 Boundary routing as a structural operator

The most significant theoretical reframing offered by this corpus is the reconceptualization of the boundary not as a simple threshold or wall, but as a *routing operator* on admissible structural regimes.

In the prior UNNS theoretical framework, the boundary $\partial\mathcal{M}_{\text{adm}}$ is characterized by what it prevents: identity-preserving trajectories cannot cross it into the HARD-fragmented exterior. This is the content of the Margin-Confinement Law. The stellar corpus adds a complementary picture: when an event is genuinely catastrophic (identity-preserving continuation fails, as in stellar collapse), the boundary does not simply stop the trajectory. Instead, it routes the residual structure into downstream admissible forms. These downstream forms each occupy the interior of $\mathcal{M}_{\text{adm}}$, but they are not the same admissible regime as the pre-boundary state, nor necessarily the same admissible regime as each other.

This routing picture is more generative than a simple wall picture. It predicts that catastrophic events should produce a *family* of post-boundary observables, each internally coherent, each admissible, but mutually non-equivalent. The number of distinct branches, their separation distances, and the routing geometry (which pre-boundary structures are nearest to which post-boundary branches) are empirically measurable through the bridge framework.

8.2 Admissible anomalies: SN2012aw

SN2012aw provides the corpus with a notable theoretical role. Across all three phases, it is the structurally extreme object: highest κ_{conn} in Phase B ($\kappa = 4.40$), highest κ_{conn} in Phase C ($\kappa = 3992$), highest TD in Phase C (TD = 0.959), and the largest branching index in the object-chain analysis (BI = 1.470).

Yet SN2012aw is FULL-percolating in every evaluation. This is the defining characteristic of a *persistent admissible anomaly*: an object that is not a failure, not excluded, not near the boundary — it is simply extreme within the admissible interior. The important theoretical shift is from the intuition that anomalies are breakdowns to the UNNS-compatible view that anomalies can be extreme admissible states near high-κ_{conn}/high-TD regions of $\mathcal{M}_{\text{adm}}$.

The object-matched incoherence of SN2012aw (its B-layer light curve is structurally closer to SN1993J's spectral series than to its own spectral series) suggests that SN2012aw is not anomalous in one observable channel only: its anomalous routing character persists across the full boundary transition. This makes it a strong candidate for detailed study in any corpus expansion.

8.3 Representation-dependent structural position

The cross-tier trajectory of the corpus (κ_{conn} : 1–2 $\rightarrow$ 0.18–4.40 $\rightarrow$ 201–3992) provides structural evidence for a general principle:

> *Structural position is not only a property of the physical object; it is a property of the object-representation pair.*

This means that a theory of admissibility cannot speak about "the system" in isolation. It must specify through which observable ladder or chart the system is being represented. The same physical event (e.g., the SN1993J collapse and its aftermath) occupies different struc-

tural coordinates when processed as a light curve ($\kappa_{\text{conn}} \approx 0.22$) versus as a spectral time series ($\kappa_{\text{conn}} = 201$). The structural complexity attributed to the event grows with the representational depth of the observable channel.

This is not merely a statement about measurement uncertainty. It is a genuine structural property: different observational representations are different ladders, and different ladders can sit in different regions of $\mathcal{M}_{\text{adm}}$.

8.4 Connections to the Admissible Cluster Geometry framework

The Admissible Cluster Geometry (ACG) manuscript [4] established that the interior of $\mathcal{M}_{\text{adm}}$ is organized into admissible basins connected by sparse continuity corridors. The present corpus adds a dynamic layer to that static picture: some admissible basins are *generated* by boundary-routing events.

In the ACG framework, the pre-collapse A-domain and the post-collapse B and C domains would appear as three distinct admissible basins: A is internally cohesive, B is internally cohesive, C is internally cohesive, but A–B, A–C, and B–C span bridge distances that cross from within-basin proximity (A–B, $d = 0.401$) to between-basin separation (B–C, A–C, $d > 1.2$). The routing event (stellar collapse) is then the mechanism by which the system transitions from the A basin to the B basin while simultaneously activating the C basin as an independent observable.

This provides a bridge from the static ACG cluster picture to a dynamical view in which basin transitions are driven by catastrophic physical events.

8.5 Broader applicability and corpus expansion

The boundary-routing pattern identified here — pre-boundary contact layer, post-boundary branching layer, orthogonal structural drivers at each transition — is not inherently specific to supernovae. The abstract pattern is:

1. a pre-boundary support state (A);
2. a first post-boundary relaxation observable (B), close to A;
3. a second post-boundary redistribution observable (C), strongly separated from both A and B.

Possible analogues in other physical domains include: the pre-stress field, seismic waveform, and aftershock field in earthquake rupture; the pre-transition material, thermal response, and structural-phase signature in a first-order phase transition; and the pre-perturbation regulatory state, population response, and molecular-expression response in biological catastrophic events.

Testing the Boundary Routing Conjecture (Conjecture 6.6) across these analogues requires constructing analogous three-layer (or multi-layer) corpora and applying the bridge framework. That is identified as a priority for Phase B and Phase C program expansion.

Within the stellar domain, immediate corpus expansion directions include: additional progenitor mass points ($15\,M_\odot$, $25\,M_\odot$, binary-stripped), additional Type II subtypes (IIn, IIL, stripped IIb vs IIP), time-resolved MESA history tracks (full stellar evolution ladder for Phase A), and an expanded spectral series covering more SNe in Phase C.

8.6 Astrophysical context and structural contribution

In astrophysics, it is well established that light curves, spectra, and progenitor structural profiles encode physically distinct information about supernova explosions. Light curves trace the integrated photometric response of the expanding ejecta; spectra encode the velocity- and ionization-state evolution of specific atomic lines; and pre-supernova radial profiles capture the final structural configuration of the stellar interior before collapse. These three observable types have long been recognized as carrying complementary but not redundant physical content.

The UNNS contribution is to quantify this non-redundancy *structurally*, through bridge geometry in the normalized structural vector space. The B–C strong separation ($d_{\mathrm{BC}} = 1.287$) provides a corpus-specific structural measure of how different the light-curve and spectral observable channels are, using the same 7-feature vector and bridge computation applied to all other UNNS domains. This does not replace astrophysical analysis of line-formation or photospheric evolution; it adds a structural-admissibility layer that is agnostic to the specific physical mechanism and therefore comparable across domains without requiring domain-specific modeling.

The pilot corpus makes no claim about progenitor-mass recovery, nucleosynthesis yields, or ejecta kinematics. Those remain the domain of radiative-transfer and hydrodynamical models. The claim is structural: that the three observable layers occupy distinct and structurally measurable positions in the bridge geometry of the UNNS vector space, and that this structural separation is consistent with the boundary-routing picture.

9 Conclusion

We have presented the Stellar Boundary Dynamics I pilot corpus: 10 STRUC-PERC-I evaluations across three observational phases of core-collapse supernovae, all returning FULL-percolation with zero HARD, GIANT, or TAIL outcomes, together with a unified ABC tri-domain bridge that classifies the routing geometry as `A_to_B_contact_with_C_branching`.

The main theoretical contribution is the **boundary-routing concept**: a catastrophic transition can preserve local structural admissibility while routing structure into non-equivalent downstream admissible regimes, rather than producing a single successor state or structural fragmentation. The pre- and post-collapse observables are each internally FULL-percolating, but they occupy structurally distinct positions in bridge space ($d_{\mathrm{AB}} = 0.401$ weak separation; $d_{\mathrm{BC}} = 1.287$, $d_{\mathrm{AC}} = 1.365$ strong separation).

The key theoretical refinement established as Proposition 6.2 is that internal FULL-percolation does not imply cross-regime structural equivalence. The bridge framework is required to determine whether connected regimes are continuous, weakly separated, or strongly separated. Together, percolation and bridge geometry provide a complete structural description of a multi-observable physical event.

Two object archetypes emerge from the corpus:

- **SN1993J** (BI = 0.504): contact-chain, compact cross-layer geometry, near-linear structural inheritance;
- **SN2012aw** (BI = 1.470): branching anomaly, escalating cross-layer displacement, FULL-percolating throughout.

The formal layer (Section 6) provides Definition 6.1 (admissible boundary-routing event), Proposition 6.2 (admissibility/equivalence separation), Theorem 6.4 (pilot corpus routing), Conjecture 6.6 (Boundary Routing), and Conjecture 6.7 (Contact-Chain/Branching-Anomaly dichotomy). These form the formal spine of the boundary-routing theory, offered with the understanding that they rest on a pilot corpus requiring expansion.

The Stellar Boundary Dynamics corpus adds to the 14-domain STRUC-PERC-I baseline a first instance of multi-layer routing geometry in a catastrophic astrophysical event, extending the UNNS program into a new theoretical territory: the study of how structure survives and reorganizes through catastrophic physical transitions.

Data and code availability. All phase summaries, normalization-review outputs, bridge comparison records, and final result files are retained in the `stellar_boundary_dynamics` corpus folder structured as described in Appendix A. Processing scripts for each pipeline stage are included alongside the data. A public archive deposit is planned; all quantitative results in this manuscript are reproducible from the data and scripts described in Appendix A.

A Reproducibility: Data Sources, Pipeline, and Output Records

This appendix documents the full processing chain, input files, conversion scripts, and output records sufficient for independent replication of the results reported in Sections 4–5.

A.1 Corpus folder structure

```
stellar_boundary_dynamics/
  A_mesa_precollapse_tracks/
  B_supernova_light_curves/
  C_spectral_time_series/
  AB_bridge/
  BC_bridge/
  ABC_bridge/
  tools/
```

Each phase folder contains: raw data, ladders, STRUC-PERC-I canonical inputs and numeric ladders, batch result CSV/JSON, alpha-application grids and vectors, normalization-review outputs, and v2 vector summaries.

A.2 Phase A: pre-supernova radial profiles

Source. Zenodo 5556959 (Laplace et al. 2021 [7]), *Different to the core: the pre-supernova structures of massive single and binary-stripped stars.*

Input files (terminal pre-SN snapshots, 128-species nuclear network).

- `profile_single_M12.09_128net.data` (`A1_12M`, 12.09 $M_\odot$, $n = 64$)
- `profile_single_M19.98_128net.data` (`A2_20M`, 19.98 $M_\odot$, $n = 64$)

Conversion scripts.

```
tools/a_presupernova_profile_to_ladder.py
tools/a_profile_ladder_to_struc_perc_i.py
tools/a_alpha_apply.py
tools/a_alpha_normalization_review.py
```

Key output files.

- `ladders/A1_12M_presupernova_profile_ladder.csv`
- `ladders/A2_20M_presupernova_profile_ladder.csv`
- `struc_perc_i/struc_perc_batch_results.csv` (STRUC-PERC-I v2.5.0)
- `alpha_application/normalization_review/A_5D_VECTOR_SUMMARY_v2.csv`

STRUC-PERC-I results. A1_12M: FULL, $\kappa_{\text{conn}} = 2$, $n = 64$, TD = 0. A2_20M: FULL, $\kappa_{\text{conn}} = 1$, $n = 64$, TD = 0.

Normalization review. Both objects: `status=review_required`. A2_20M composition/gap = 254.5×. Bridge comparison uses `A_5D_VECTOR_SUMMARY_v2.csv`.

A.3 Phase B: supernova light curves

Source. Open Supernova Catalog / AstroCats [8]. Six objects: SN1987A, SN1993J, SN1999em, SN2011dh, SN2012aw, SN2013ej.

Conversion scripts.

```
tools/osc_to_b_ladder.py
tools/b_ladder_to_struc_perc_i.py
tools/b_struc_input_to_numeric_ladders.py
tools/b_alpha_apply.py
tools/b_alpha_normalization_review.py
```

Key output files.

- `ladders/B_{SN1987A,...,SN2013ej}_light_curve_ladder.csv`
- `struc_perc_i/struc_perc_batch_results.csv`
- `alpha_application/normalization_review/B_5D_VECTOR_SUMMARY_v2.csv`

STRUC-PERC-I results (all FULL).

Object	κ_{conn}	n (rungs)	TD
SN1987A	0.422	34	0.000
SN1993J	0.422	37	0.000
SN1999em	0.178	36	0.000
SN2011dh	1.000	45	0.000
SN2012aw	4.400	80	0.329
SN2013ej	0.316	95	0.000

Normalization review. SN1987A: comparable. SN1993J, SN1999em, SN2011dh, SN2012aw, SN2013ej: review_required (curvature-channel dominance ranging from 10× to 699,671×). Bridge uses `B_5D_VECTOR_SUMMARY_v2.csv`.

A.4 Phase C: spectral time series

Source. WISeREP [9]. Spectral line-window proxies for 8 targeted lines: Hα, Hβ, He I 5876, O I 7774, Ca II NIR, Si II 6355, Fe II 5169, Ni/Co decay proxy.

Conversion scripts.

```
tools/c_spectra_to_line_ladder.py
tools/c_line_ladder_to_struc_perc_i.py
tools/c_alpha_apply.py
tools/c_alpha_normalization_review.py
```

Key output files.

- `ladders/C1_SN1993J_spectral_line_ladder.csv` (685 rows; 99 spectra; 8 lines)
- `ladders/C2_SN2012aw_spectral_line_ladder.csv` (560 rows; 84 spectra; 8 lines)
- `struc_perc_i/struc_perc_batch_results.csv`
- `alpha_application/normalization_review/C_5D_VECTOR_SUMMARY_v2.csv`

STRUC-PERC-I results. C1 (SN1993J): FULL, $\kappa_{\text{conn}} = 201.4$, $n = 685$, TD = 0.570. C2 (SN2012aw): FULL, $\kappa_{\text{conn}} = 3992.4$, $n = 198$, TD = 0.959.

Normalization review. Both objects: review_required, max_channel=flux. C2_SN2012aw: high_tail_attention, high_kappa_attention. Bridge uses `C_5D_VECTOR_SUMMARY_v2.csv`.

A.5 Bridge runs

Scripts.

```
tools/ab_bridge_compare.py
tools/bc_bridge_compare.py
tools/abc_bridge_compare.py
```

ABC bridge run command.

```
python tools/abc_bridge_compare.py \
  ABC_bridge/inputs/A_5D_VECTOR_SUMMARY_v2.csv \
  ABC_bridge/inputs/B_5D_VECTOR_SUMMARY_v2.csv \
  ABC_bridge/inputs/C_5D_VECTOR_SUMMARY_v2.csv \
  ABC_bridge
```

Output records.

- `AB_bridge/summaries/AB_BRIDGE_RESULT_RECORD.txt`
- `BC_bridge/summaries/BC_BRIDGE_RESULT_RECORD.txt`
- `ABC_bridge/summaries/ABC_BRIDGE_RESULT_RECORD.txt`
- `ABC_bridge/comparisons/ABC_DOMAIN_CENTROID_COMPARISON.csv`
- `ABC_bridge/comparisons/ABC_OBJECT_CHAIN_ALIGNMENT.csv`

ABC bridge features. `mean_GR`, `var_GR`, `anisotropic_persistence_bounded`, `admissibility_persistence`, `collapse_onset_radius`, `kappa_connect_reference`, `tail_dominance_reference` (7 features; v2 normalized).

Instrument. STRUC-PERC-I v2.5.0 for all 10 evaluations. All batch result files: `struc_perc_batch_results.csv` + `struc_perc_batch_results.json` in each phase's `struc_perc_i/` subfolder.

References

[1] UNNS Substrate Research Program. The Universal Structural Law: Admissibility Bounds on Ordered Physical Systems. *UNNS Working Manuscript*, 2026.

[2] UNNS Substrate Research Program. The Percolative Realizability Principle: Connectivity Margin as a Coordinate of Realizability Space. *UNNS Working Manuscript*, 2026.

[3] UNNS Substrate Research Program. The Margin-Confinement Law: Structural Non-Crossability in Admissibility Space. *UNNS Working Manuscript*, 2026.

[4] UNNS Substrate Research Program. Admissible Cluster Geometry: Recoverable Connectivity in Realizability Space. *UNNS Working Manuscript*, 2026.

[5] UNNS Substrate Research Program. Beyond Fragmentation: The Forced Coherent Collapse Regime and Unified Tail Dominance Scaling. *UNNS Working Manuscript*, 2026.

[6] UNNS Substrate Research Program. Local Geometry of Realizability Boundaries: Bi-Lipschitz Distance Representation. *UNNS Working Manuscript*, 2026.

[7] M. Laplace, Y. Götberg, S. E. de Mink, E. Zapartas, and R. Farmer. The after-lives of single and binary star evolution: compact remnants, and supernova ejecta of stars up to 350 $M_\odot$. *Astronomy & Astrophysics*, 656:A58, 2021. https://doi.org/10.5281/zenodo.5556959

[8] G. Guillochon, J. Parrent, L. Z. Kelley, and R. Margutti. An Open Catalog for Supernova Data. *The Astrophysical Journal*, 835(1):64, 2017.

[9] O. Yaron and A. Gal-Yam. WISeREP — An Interactive Supernova Data Repository. *Publications of the Astronomical Society of the Pacific*, 124(917):668, 2012. https://www.wiserep.org/ https://ui.adsabs.harvard.edu/abs/2012PASP..124..668Y/abstract